

Reduction of nitrophenols to aminophenols under concerted catalysis by Au/g-C₃N₄ contact system

Yongsheng Fu ¹, Ting Huang ¹, Bingquan Jia, Junwu Zhu ^{*}, Xin Wang ^{*}

Key Laboratory of Soft Chemistry and Functional Materials, Nanjing University of Science and Technology, Ministry of Education, Nanjing 210094, China

ARTICLE INFO

Article history:

Received 30 June 2016

Received in revised form

13 September 2016

Accepted 24 September 2016

Available online 28 September 2016

Keywords:

Contact system

g-C₃N₄

Au nanoparticles

Concerted catalysis

Induced charge-transfer effect

ABSTRACT

We report a facile one-step strategy to fabricate an Au/g-C₃N₄ contact system with different Au contents. Morphology observation shows that Au nanoparticles with an average diameter of 2.6 nm are firmly anchored on the surface of two-dimensional g-C₃N₄ sheets. It is found that the Au/g-C₃N₄ contact system exhibits an unusual bi-functionality of catalytic and visible-light-driven photocatalytic activities, thus the hydrogenation reduction of nitrophenol to aminophenol can be rapidly achieved under concerted catalysis by the system. Among the Au/g-C₃N₄ contact systems studied, the Au/g-C₃N₄-6 exhibits the highest rate constant of $5.9362 \times 10^{-3} \text{ s}^{-1}$ in the dark and $7.9895 \times 10^{-3} \text{ s}^{-1}$ under visible light irradiation for the reduction of *p*-nitrophenol to *p*-aminophenol, which is impressively higher than that pure Au nanoparticles or recently reported Au-based nanocatalysts. Such a concerted catalysis can be attributed to the negative shift in Fermi level of Au caused by the induced charge-transfer effect as a result of the strong interaction between Au nanoparticles and g-C₃N₄.

© 2016 Elsevier B.V. All rights reserved.

1. Introduction

Gold nanoparticles (Au NPs) are the most stable metal nanoparticles and they exhibit size-dependent unique properties that differ from those of bulk gold due to the quantum confinement effect, exceedingly large surface-to-volume ratio and more negative Fermi potential [1–5]. Applications of Au NPs to catalysis, biology and other fields have received great interest [6–13]. However, gold is a rare and precious metal and Au NPs alone usually suffer from serious agglomeration, leading to the rapid decay of catalytic activity and the poor durability of the catalyst. To stabilize the nanocatalyst system, enhance the catalytic performance and reduce the production costs, gold may be alloyed with other metals to give it special properties [14–18], while various support materials, such as metal oxide [19–23], carbonaceous materials and polymers [24–29], have been used to disperse ultra-fine Au NPs. Among these hybrid systems, Au-semiconductor contact system have been constructed and applied to many fields. Au-TiO₂ nanocatalysts showed high catalytic activity for specific reactions in dark conditions such as CO oxidation [30]. The Au/TiO₂ Schottky contact

exhibited superior photocatalytic activity in dye decomposition and water-reduction hydrogen production under visible-light illumination [31]. The ternary Au-CeO₂-TiO₂ system showed excellent and stable photocatalytic activity for NO abatement [9]. The Au/CdS system prepared via reductive deposition method was reported as a high-performance catalyst for photocatalytic hydrogen production [32]. It has been demonstrated that in the semiconductor-based solar energy conversion process, the metal-semiconductor contact with the differing work function can significantly influence the photocatalytic efficiency of semiconductor photocatalyst via the induced charge-transfer mechanism [11,31].

Graphitic carbon nitride (g-C₃N₄), as a sustainable and environmentally friendly metal-free semiconductor, possesses a graphene-like two dimensional (2D) crystalline structure, remarkable chemical and thermal stability and suitable band gap (2.7 eV) for sunlight absorption. These characteristics make g-C₃N₄ an ideal candidate for applications like visible-light-driven photocatalytic water splitting, CO₂ reduction, organic pollutant degradation and organic synthesis [33–35].

It is known that electron-hole pairs can be produced under light irradiation and may travel between the metal-semiconductor interface to form a positively charged region and a negatively charged region because of the Schottky effect [11]. Because of the great importance of photocatalysis, most studies have focused on the influence of the metal nanoparticles on the semiconductor, how-

* Corresponding authors.

E-mail addresses: zhujw@njust.edu.cn, wxin48@163.com (J. Zhu), wangx@njust.edu.cn, wxin48@163.com (X. Wang).

¹ These authors contributed equally to this work.

ever, relatively little attention has been paid so far to the effect of the semiconductor on the catalytic activity of metal nanoparticles. Recently, Li et al. reported that the mesoporous g-C₃N₄ nanorod- metal nanoparticles system exhibited a high photocatalytic activity for the hydrogen generation from water by using triethanolamine (TEA) as a sacrificial electron donor and for the reduction of nitrophenol with tandem catalysis in one step [36]. We prepared a Pd/g-C₃N₄ system, which showed superior catalytic activity in Suzuki–Miyaura coupling reactions and an Ag/g-C₃N₄ metal-semiconductor for catalytic/photocatalytic degradation of dyes [37,38]. It is known that nitrophenols are very important starting materials for producing aminophenols and other chemicals but considered to be implicated in carcinogenesis. On the other hand, aminophenols with lower toxicity can be widely used as intermediates for the manufacture of many fine chemicals [39–42]. Therefore, to explore new catalysts with high activity for the reduction of nitrophenols to aminophenols is valuable for both of the industrial processes and environmental protection.

Herein, we report a facile one-step strategy for the synthesis of Au/g-C₃N₄ contact system with different Au contents. The Au/g-C₃N₄ system exhibits high rate constants in the dark or under visible light irradiation for the reduction of *p*-nitrophenol to *p*-aminophenol, which are superior to pure Au NPs or recently reported Au-based nanocatalysts. Consequently, the hydrogenation reduction of *p*-nitrophenol to *p*-aminophenol can be rapidly achieved under concerted catalysis by the Au/g-C₃N₄ contact system.

2. Experimental

2.1. Synthesis of Au/g-C₃N₄ contact system

All chemicals were of reagent grade and used without further purification. Ultrapure water was obtained from a Millipore purification system. The g-C₃N₄ nanosheets were synthesized as described in the previous report [38]. The Au/g-C₃N₄ contact system with differing Au contents (1, 2, 3, 4, 5, 6, 8 wt%) were prepared and labeled as Au/g-C₃N₄-x (x=1, 2, 3, 4, 5, 6, 8). A typical experiment for the synthesis of Au/g-C₃N₄-1 catalyst is as follows: 100 mg of the as-prepared g-C₃N₄ nanosheets were added into 150 mL ultrapure water under ultrasonic irradiation for 30 min. After that, HAuCl₄ (1 mg of Au) was dissolved in the g-C₃N₄ nanosheets dispersion and stirred for 30 min at the room temperature. Then the freshly prepared NaBH₄ solution (20 μL, 0.3 g mL⁻¹) was slowly added into the above solution with continuous stirring for 60 min, inducing a distinct color change from yellow to amaranth. The mixture was heated to 60 °C for 3 h with constant stirring and cooled to the room temperature. Finally, the Au/g-C₃N₄-1 nanocomposite was obtained after freeze drying.

2.2. Characterization

The powder X-ray diffraction (XRD) spectra were recorded on a Bruker D8 Advanced diffractometer with Cu Kα radiation ($\lambda = 1.5418 \text{ \AA}$) and the scanning angle ranged from 5° to 80° of 2θ. Fourier transform-infrared (FT-IR) spectra of the samples were carried out on a Bruker VECTOR 22 spectrometer using the KBr pellet technique. The X-ray photoelectron spectroscopy (XPS) analysis was performed on a RBD upgraded PHI-5000C ESCA system (Perkin Elmer) with Mg K radiation ($h = 1253.6 \text{ eV}$). All binding energies were internally referenced to the C 1s peak (284.6 eV). The Au content in the Au/g-C₃N₄ contact system was analyzed by inductively coupled plasma atomic emission spectrometry (ICP-AES, Shimadzu ICP-7510). Transmission electron microscopy (TEM) images, high-resolution transmission electron microscopy (HRTEM) images and

scanning transmission electron microscopy (STEM) images were taken on a JEOL-2100 microscope with an accelerating voltage of 200 kV. Photocurrent measurements were carried out on a CHI 660D electrochemical workstation in a standard three-electrode system using the prepared samples as the working electrodes with an active area of ca. 0.5 cm², platinum foil as the counter electrode, and a saturated calomel electrode (SCE) as the reference electrodes, respectively. Photocurrent measurements were performed in 1 M Na₂SO₄ by using 500 W xenon lamp with a 420 nm cutoff filter (the average light intensity was 31.2 mW cm⁻²) as the source of visible light irradiation.

2.3. Evaluation of the catalytic activity of Au/g-C₃N₄

The catalytic activity of the as-obtained Au/g-C₃N₄ contact system was evaluated by the catalytic hydrogenation reactions of nitrophenols at room temperature (25 °C) in the dark. The experimental procedure is as follows: 1.0 mg of Au/g-C₃N₄ contact system solution was added into 50 mL *p*-nitrophenol (*p*-NP) aqueous solution with a concentration of 10 mg L⁻¹ under magnetic stirring, followed by a continuous purge with N₂ for 20 min to remove the dissolved O₂. After that, 75 μL of freshly prepared NaBH₄ solution (0.1 g mL⁻¹) was injected directly into above mixture under continuous stirring to initiate the reaction. To monitor the reaction progress, at a given time interval of 2 min, 5 mL aliquots were collected and then filtered to remove the catalyst. The catalytic hydrogenation reactions of nitrophenols over Au/g-C₃N₄ contact system were performed in quartz constant temperature bath (25 °C) under visible-light irradiation. Photo-irradiation was carried out using a 500 W xenon lamp with UV cut-off filters (JB450) to completely remove any radiation below 420 nm and to ensure illumination by visible-light only. The concentrations of *p*-NP in the as-obtained clear liquid were measured by a UV-vis spectroscopy at the absorbance of 400 nm. After the reaction, the reaction mixture was extracted with ethyl acetate and was detected by gas chromatography coupled with mass spectrometry (GC-MS) using an Agilent 7890A/5975C. In order to further confirm the effect of Au/g-C₃N₄ contact system on enhancement the catalytic activity of Au, *o*-nitrophenol (*o*-NP), *m*-nitrophenol (*m*-NP), 2,4-dinitrophenol (2,4-DNP) and 2,4,6-trinitrophenol (2,4,6-TNP) were also conducted under the same conditions. The catalytic stability and reusability of the Au/g-C₃N₄ contact system have been evaluated. The catalytic activity measurements were performed for 10 cycles under the same reaction conditions. After each cycle, the all catalysts were separated from the reaction mixture by a simple filtration, washed with deionized water, and reused for the next cycle.

2.4. Structure and morphology

The typical XRD patterns of the as-prepared pure g-C₃N₄ and Au/g-C₃N₄-6 contact system are shown in Fig. 1(a). The pure g-C₃N₄ gives two diffraction peaks: the most intense peak at 27.5° with d-spacing value of 0.326 nm can be assigned to the (002) plane of graphitic stacking g-C₃N₄, while the peak at 13.00° with d-spacing value of 0.68 nm can be indexed as (100), which belongs to an in-plane structural packing motif between nitride pores[43,44]. After the anchoring of Au nanoparticles, the diffraction intensity of (100) crystal plane of g-C₃N₄ was distinctly decreased. Two weak peaks can be observed at 38.2° and 44.4°, ascribable to the Au (111) and (200) crystal planes with a face-centered cubic structure, respectively [3,45,46].

Fig. 1(b) presents the FTIR spectra of pure g-C₃N₄ and Au/g-C₃N₄-6 contact system. It can be clearly seen that pure g-C₃N₄ and Au/g-C₃N₄-6 exhibit almost the same IR features in the whole spectra. The broad peaks between 3000 and 3500 cm⁻¹ are originated

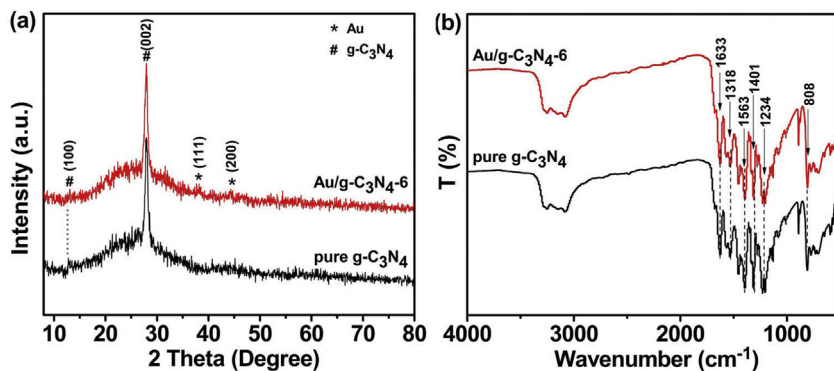


Fig. 1. (a) XRD diffraction patterns and (b) FT-IR spectra of pure g-C₃N₄ and Au/g-C₃N₄-6 contact system.

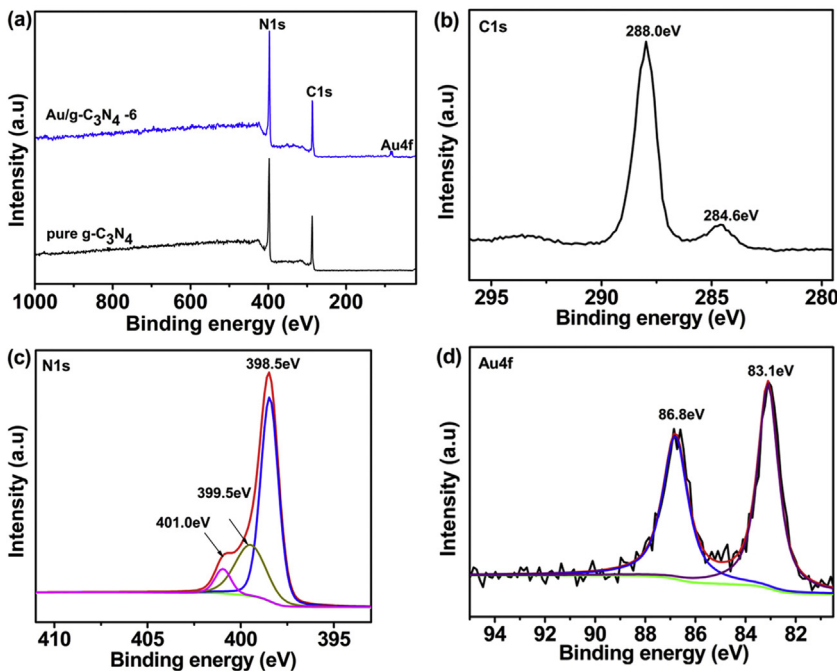


Fig. 2. XPS survey spectra of g-C₃N₄ and Au/g-C₃N₄-6 (a); high resolution C 1s (b) and N 1s (c) and Au 4f (d) spectra of Au/g-C₃N₄-6.

from the stretching vibration N—H and that of O—H of the physically adsorbed water. The peaks in the region from 1000 to 1800 cm⁻¹ can be attributed to the characteristic stretching modes of CN heterocycles. The sharp peak at around 808 cm⁻¹ is contributed by the typical breathing mode of triazine units [42–45].

The elemental composition and the oxidation state of the elements of the samples were analyzed by XPS. As observed from Fig. 2(a), the survey spectrum of Au/g-C₃N₄-6 reveals the co-existence of C, N and Au in the sample. High-resolution spectra for C 1s, N 1s and Au 4f of Au/g-C₃N₄-6 are depicted in Fig. 2(b-d), respectively. In the C 1s spectrum, the peaks at 284.6 eV and 288.0 eV can be ascribed to the sp²-hybridized adventitious carbon atom and the carbon atom (N=C—N₂) in the triazine ring of g-C₃N₄, respectively. The N 1s spectrum in Fig. 2(c) can be fitted into three peaks with binding energies of 398.5, 399.5 and 401.0 eV, ascribable to the sp²-hybridized nitrogen atom (C=N=C) in the triazine ring, sp³-hybridized nitrogen atom (N—(C)₃) and (C—N—H), respectively [42–45]. As shown in Fig. 2(d), the two peaks located at 86.8 eV and 83.1 eV originated from Au 4f_{5/2} and Au 4f_{7/2}, well in agreement with metallic Au [23,46]. Elementary analysis of ICP-AES shows that the weight percentages (wt%) of Au in the prepared Au/g-

C₃N₄-1, Au/g-C₃N₄-2, Au/-C₃N₄-3, Au/g-C₃N₄-4, Au/g-C₃N₄-6 and Au/g-C₃N₄-8 are 0.82, 1.75, 2.38, 3.03, 4.35 and 5.56 wt%, respectively.

The morphology and size distribution of the supported Au NPs on g-C₃N₄ sheets were characterized by TEM and STEM. As shown in Fig. 3(a), the monodispersed Au NPs are uniformly anchored on the surface of g-C₃N₄ with a two-dimensional sheet-like morphology. HRTEM image of Au/g-C₃N₄-6 (the inset of Fig. 3(a)) typically exhibits the characteristic lattice fringes with crystal plane distances of 0.235 nm, which can be indexed to the spacing of the (111) planes in face-centered cubic (fcc) of Au nanoparticles, in accordance with the XRD results. As can be seen from Fig. 3(b), the average diameter of Au NPs is 2.6 nm with a narrow particle size distribution. Fig. 3(c) shows the high angle annular dark field STEM images of the as-prepared Au/g-C₃N₄-6, while the elemental mapping (Fig. 3(d)) demonstrates that C, N and Au elements are homogeneously dispersed in the Au/g-C₃N₄ contact system. Fig. 1S displays the nitrogen adsorption-desorption isotherms of pure g-C₃N₄ and Au/g-C₃N₄-6 contact system. The specific surface area of Au/g-C₃N₄-6 contact system (58.9 m² g⁻¹) is about 1.7 times as high as that of the pure g-C₃N₄ (34.8 m² g⁻¹).

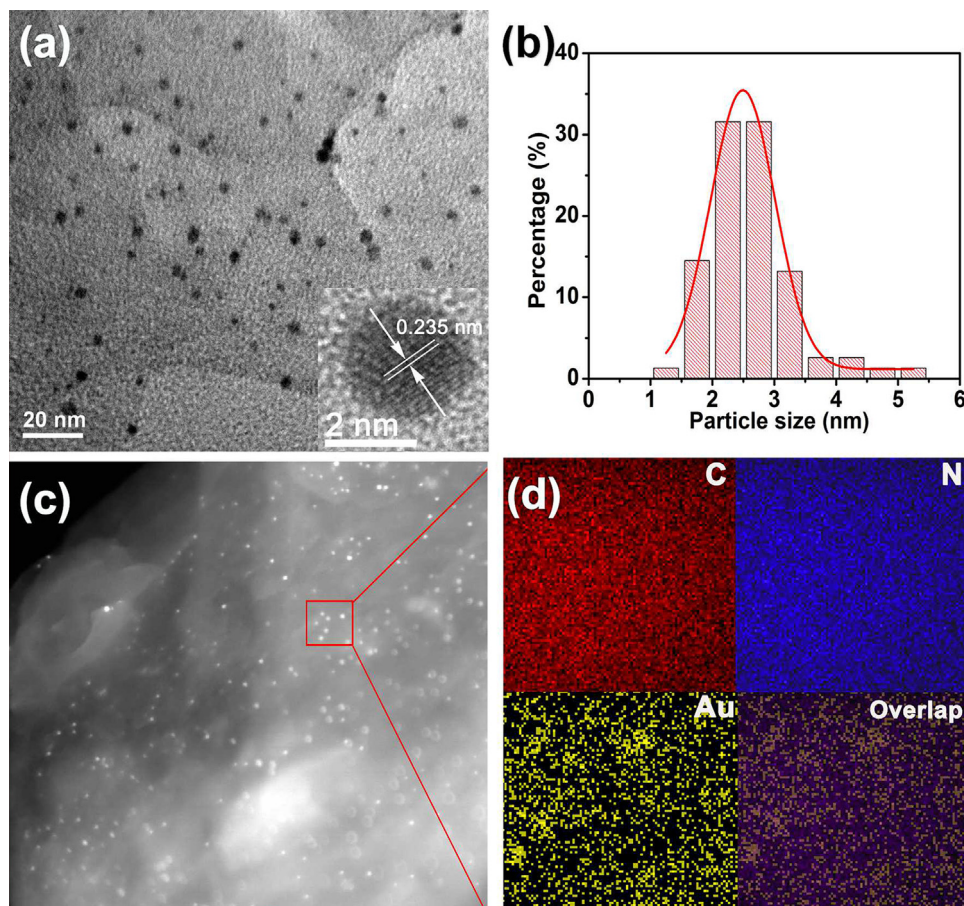


Fig. 3. TEM image (a), Histogram of Au particle size distribution (b), STEM image (c) and the elemental mapping images of C, N and Au elements (d) of the Au/g-C₃N₄-6 contact system.

2.5. Catalytic activity of Au/g-C₃N₄ contact system for nitrophenols hydrogenation reactions

The catalytic reduction of *p*-nitrophenol to *p*-aminophenol by NaBH₄ was chosen as a model reaction to evaluate the catalytic activities of the Au/g-C₃N₄ contact system. Fig. 4(a) shows the time-dependent absorption of *p*-nitrophenol and *p*-aminophenol in the presence of Au/g-C₃N₄-6 contact system and excess NaBH₄. It is widely known that the wavelength of maximum absorption of *p*-nitrophenol solution is centered at 317 nm in neutral or acidic condition and shifts to 400 nm after treatment with freshly prepared NaBH₄ due to the formation of *p*-nitrophenolate ions in alkaline media caused by the addition of NaBH₄ [47,48]. After adding the Au/g-C₃N₄-6 contact system, the peak at 400 nm rapidly decreased while the typical absorption of *p*-aminophenol at 300 nm appeared and then increased obviously. The initially light yellow solution became colorless within 10 min, indicating that almost all the *p*-nitrophenol molecules in the solution were reduced to *p*-aminophenol. Fig. 4(b) presents time profiles of C/C₀ using different catalysts, where C and C₀ are the concentrations of *p*-nitrophenolate at the reaction time t and 0, respectively. It can be clearly seen that the pure g-C₃N₄ alone is catalytically inactive for the reduction of *p*-nitrophenol while the unsupported Au NPs exhibits a limited catalytic activity for the hydrogenation reduction. The blank experiment has been carried out and the results are shown in Fig. 2S. It can be clearly seen that NaBH₄ alone cannot reduce nitrophenols to aminophenols with or without visible light irradiation, which is in accordance with the result of reference [49]. It is interesting that the combination of Au NPs and g-C₃N₄ sheets

can lead to higher catalytic performances and the activity varies according to the Au content in Au/g-C₃N₄ contact system, among the catalysts with different Au content, the catalytic reduction of *p*-nitrophenol over the Au/g-C₃N₄-6 contact system showed the highest conversion within 10 min, accordingly, the Au/g-C₃N₄-6 was selected as the optimized catalyst. Considering the initial concentration of NaBH₄ far exceeds that of *p*-nitrophenol (~15 times) and the reduction rate can be regarded to be independent from the concentration of NaBH₄. Accordingly, the reaction process can be described as the pseudo-first-order kinetics with respect to the concentration of *p*-nitrophenol and the rate constant (*k*) can be calculated according to Eq. (1)

$$k = \frac{1}{t} \ln \frac{C}{C_0} \quad (1)$$

where C and C₀ are the concentrations of *p*-nitrophenolate at the reaction time t and 0, respectively. Fig. 4(c) displays a linear relationship of ln(C/C₀) vs. time based on the experimental results, confirming that the catalytic reduction of *p*-nitrophenol to *p*-aminophenol over Au/g-C₃N₄ catalysts follow the pseudo-first-order kinetics. Among these catalysts, Au/g-C₃N₄-6 showed the highest rate constant of 5.9362 × 10⁻³ s⁻¹ (Table 1).

It is worth noting that the reduction reaction can be greatly accelerated under visible light irradiation. Fig. 4(d) shows that the *p*-nitrophenol molecules could be completely reduced to *p*-aminophenol over Au/g-C₃N₄-6 contact system within 8 min without any side reaction. GC-MS analysis also showed that all *p*-nitrophenols were fully converted to *p*-aminophenol and no by-products were detected after the reaction (Fig. 3S, Table 1S). Similar results were obtained for all the Au/g-C₃N₄ catalysts with differing

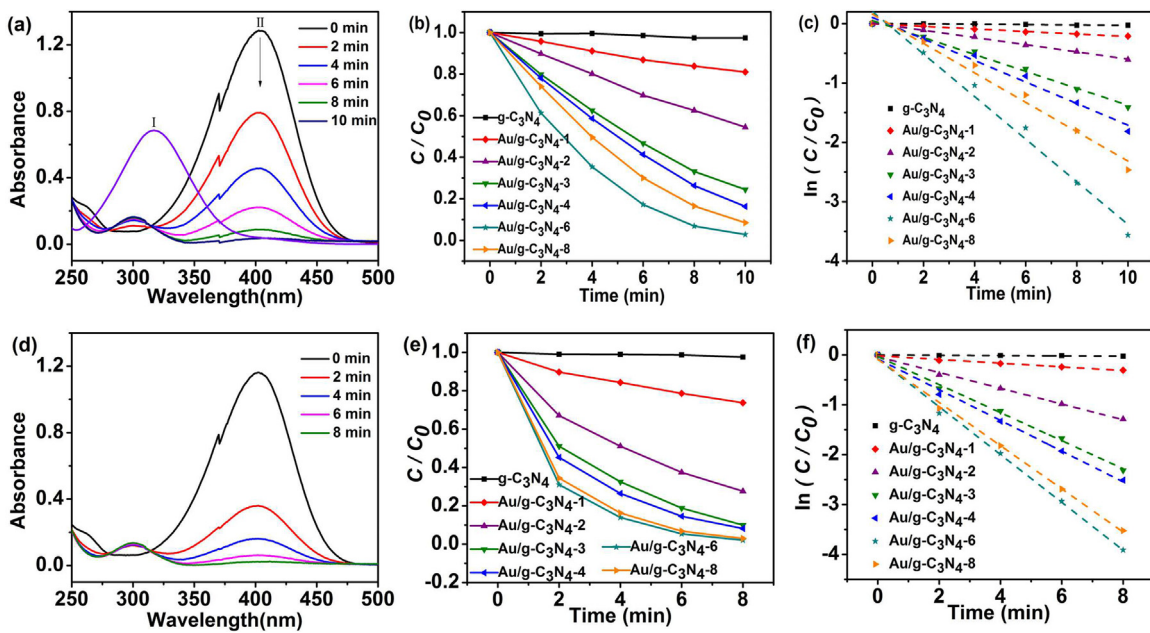


Fig. 4. Time-dependent UV-vis absorption spectra for the catalytic reduction of *p*-nitrophenol to *p*-aminophenol over the Au/g-C₃N₄-6 contact system in the presence of NaBH₄ in the dark (a) and under visible light irradiation (d); Plots of C/C₀ versus reaction time and ln(C/C₀) versus reaction time for the catalytic reduction of *p*-nitrophenol to *p*-aminophenol over different catalysts in the presence of NaBH₄ in the dark (b) and (c) and under visible light irradiation (e) and (f), respectively.

Table 1

The rate constants of the pseudo-first-order kinetics of the catalytic reduction of *p*-nitrophenol to *p*-aminophenol over different Au/g-C₃N₄ contact system in the presence of NaBH₄ in the dark and under visible light irradiation.

Samples	The rate constant of pseudo-first-order kinetics (k, 10 ⁻³ s ⁻¹)	
	In the dark	Under visible light irradiation
g-C ₃ N ₄	0.0445	0.0457
Au/g-C ₃ N ₄ -1	0.3515	0.6180
Au/g-C ₃ N ₄ -2	1.0135	2.6310
Au/g-C ₃ N ₄ -3	2.3485	4.6885
Au/g-C ₃ N ₄ -4	3.0270	5.1328
Au/g-C ₃ N ₄ -6	5.9362	7.9895
Au/g-C ₃ N ₄ -8	4.4417	7.2192

Au contents under visible light irradiation (Fig. 4(e)). The conversion rate of *p*-nitrophenol to *p*-aminophenol over Au/g-C₃N₄ contact system is well consistent with the pseudo-first-order kinetics model and the Au/g-C₃N₄-6 contact system gives the highest rate constant of 7.9895 × 10⁻³ s⁻¹ (Fig. 4(f) and Table 1), which is about 1.4 times as high as that of the Au/g-C₃N₄-6 contact system without visible light irradiation. This interesting phenomenon implies that the reduction of *p*-nitrophenols to *p*-aminophenols can be more effectively achieved under the concerted catalysis by Au/g-C₃N₄ contact system.

The catalyst turnover number (TON) and turnover frequency (TOF) can be used for assessing catalytic efficiency [47,50]. In heterogeneous catalysis, TON is usually defined as the absolute number of passes through the catalytic cycle before the catalyst becomes deactivated while TOF as the number of passes through the catalytic cycle per unit time. A comparison of the recently reported results on catalytic reduction of *p*-nitrophenol to *p*-aminophenol over different Au-based catalysts is summarized in Table 2. It can be seen that Au/g-C₃N₄-6 contact system exhibits more superior catalytic efficiency with an average TOF = 115.7 h⁻¹ for the reaction under visible light irradiation for 8 min even with the lowest catalyst dosage.

Fig. 5(a) shows the effect of the dosage of NaBH₄ on the catalytic reduction over Au/g-C₃N₄-6 contact system. It can be seen that the reaction rates of the catalytic reduction of *p*-nitrophenol

Table 2

The catalytic efficiency of different catalysts for catalytic reduction of *p*-nitrophenol to *p*-aminophenol.

Samples	Au (mol%)	Size Au (nm)	NaBH ₄ (equiv.)	TOF (h ⁻¹)	Reference
AuNPs/SNTs	27	3–5	42	46	[39]
Au/PDMAEMA-PS	700	4.2	57	1	[40]
Au/Boehmite	270	15–40	100	0.69	[41]
α-CD-capped Au	16.6	10–50	42	34	[42]
Au/g-C ₃ N ₄ -6	6.14	2.6	15	115.7	This work

Table 3

The catalytic efficiency of Au/g-C₃N₄-6 contact system for catalytic reduction of *o*-NP, *m*-NP, *p*-NP, 2,4-DNP and 2,4,6-TNP.

Different NP	Time (min)	TON	TON (h ⁻¹)
<i>o</i> -NP	6	15.059	150.6
<i>m</i> -NP	6	15.350	153.5
<i>p</i> -NP	8	15.420	115.7
2,4-DNP	10	12.492	74.9
2,4,6-TNP	10	8.056	48.3

to *p*-aminophenol were significantly increased by increasing the dosage of NaBH₄ in the range of 20–75 μL, however, the dosage of 150 μL did not give an obviously higher rate constant value than that of 75 μL, thus 75 μL of NaBH₄ was used in all experiments.

As shown in Fig. 5(b), the Au/g-C₃N₄ contact system can be easily separated by filtration and reused under the same reaction conditions, and the reduction rate of *p*-nitrophenol to *p*-aminophenol can maintain over 95% after ten cycles, revealing the high stability and reusability of the resulting Au/g-C₃N₄ contact system.

To further study the universality and practicability of the Au/g-C₃N₄ contact system, catalytic reduction of more nitrophenols, such as *o*-nitrophenol (*o*-NP), *m*-nitrophenol (*m*-NP), 2,4-dinitrophenol (2,4-DNP) and 2,4,6-trinitrophenol (2,4,6-TNP) was also carried out under the same conditions. As shown in Fig. 6 and Table 3, the Au/g-C₃N₄-6 contact system exhibited remarkable catalytic activity and the reduction rate for the nitrophenols under visible light irradiation, which follow the order: *m*-NP > *o*-NP > *p*-NP > 2,4-DNP > 2,4,6-TNP.

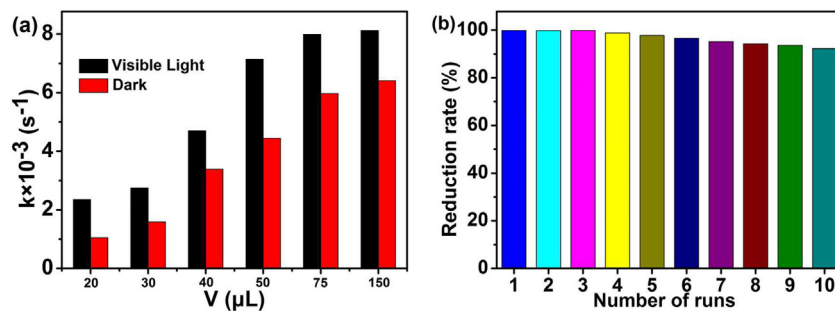


Fig. 5. (a) Rate constant values (k) of the catalytic reduction of *p*-nitrophenol to *p*-aminophenol over Au/g-C₃N₄-6 contact system with different dosage of NaBH₄ in the dark and under visible light irradiation; (b) The recycling stability of Au/g-C₃N₄-6 contact system for catalytic reduction of *p*-nitrophenol to *p*-aminophenol.

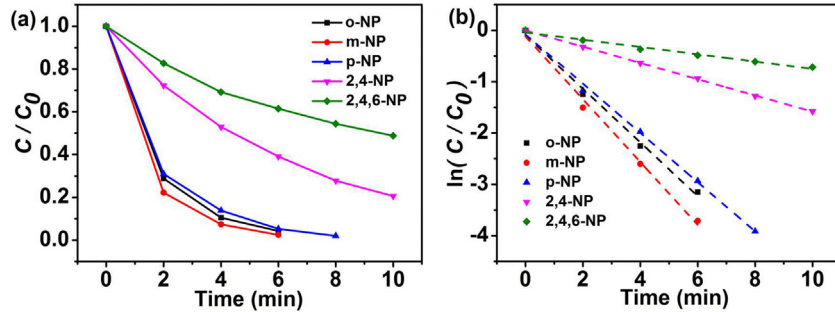


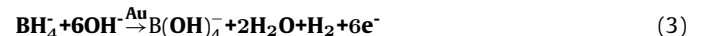
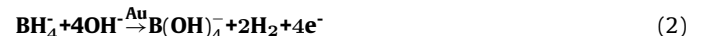
Fig. 6. (a) Plots of C/C_0 versus reaction time and (b) $\ln(C/C_0)$ versus reaction time for the catalytic reduction of *o*-nitrophenol (*o*-NP), *m*-nitrophenol (*m*-NP), *p*-nitrophenol (*p*-NP), 2,4-dinitrophenol (2,4-DNP) and 2,4,6-trinitrophenol (2,4,6-TNP) over Au/g-C₃N₄-6 contact system in the presence of NaBH₄ under visible light irradiation, respectively.

2.6. The mechanism of the reduction of nitrophenols under concerted catalysis by Au/g-C₃N₄ contact system

The above experimental results clearly demonstrate that the Au/g-C₃N₄ contact system possesses an unusual bi-functionality of catalytic and photocatalytic activities for the reduction of *p*-nitrophenol to *p*-aminophenol. Such a concerted catalysis can be attributed to the negative shift in Fermi level of Au caused by the induced charge-transfer effect as a result of the strong interaction between Au NPs and g-C₃N₄. A possible mechanism for the concerted catalysis by Au/g-C₃N₄ contact system is proposed as in Fig. 7.

It is known that the work function is the minimum energy needed to remove an electron from the Fermi level into vacuum [11,51,52]. As can be seen from Fig. 7(a), Au NPs possess a work function of $\Phi_{\text{Au}} = 5.3 \text{ eV}$ [53], which is much higher than that of g-C₃N₄ ($\Phi_{\text{g-C}_3\text{N}_4} = 4.3 \text{ eV}$) [52]. Upon intimate contact of Au nanoparticles and g-C₃N₄, there is a potential barrier for electrons to cross from Au NPs to the g-C₃N₄, which exhibits the rectifying behavior of Schottky contact. As a result, the Fermi level of Au nanoparticles shifts to more negative potential until an equilibrium is reached between Au and g-C₃N₄ (Fig. 7(b)), implying that the catalytic activity of Au/g-C₃N₄ contact system is more efficient than that of single Au nanoparticles. This result can be further confirmed by comparative experiments (Fig. 8(a and b)) and the rate constant over Au/g-C₃N₄-6 contact system ($5.9362 \times 10^{-3} \text{ s}^{-1}$) is almost five times as high as that over pure Au ($1.1943 \times 10^{-3} \text{ s}^{-1}$). Under visible light irradiation (Fig. 7(c)), electrons (e^-) in the valence band (VB) of g-C₃N₄ were excited to the conduction band (CB), followed by rapid transfer of photogenerated electrons from CB of g-C₃N₄ to the Au nanoparticles which have a strong ability to store electrons. With the continuously increasing of electron density within the Au NPs, Fermi level of Au NPs shifts toward more negative potential until it close to the CB of g-C₃N₄ where electrons possess extremely strong reducibility, thereby further enhancing the catalytic activity of Au/g-C₃N₄ contact system (Fig. 8(c and d)) [51].

Transient photocurrent measurements were carried out to study the transfer mechanism of photogenerated carriers for the Au/g-C₃N₄ contact system. The photocurrent responses of the Au/g-C₃N₄-6 electrode were recorded for five on-off cycles under visible light irradiation. As shown in Fig. 9, the Au/g-C₃N₄-6 electrode gave a photocurrent response of $0.018 \mu\text{A}$, much smaller than that of our previously reported Ag/g-C₃N₄ electrode ($0.25 \mu\text{A}$), which is attributed to the remarkable electron-storing capacity of Au NPs [51]. It is interesting that the photocurrent response of Au/g-C₃N₄-6 electrode can be prominently enhanced in the presence of NaBH₄. Au/g-C₃N₄-6 electrode exhibited a photocurrent response of $0.12 \mu\text{A}$ even in the dark because of the oxidation of BH₄⁻ with electrons being released along with H₂ gas on the Au nanoparticles (Eq. (2)) [54]. The photocurrent response of Au/g-C₃N₄-6 electrode was further enhanced to $0.22 \mu\text{A}$ under visible light irradiation due to more negative Fermi level potential of Au nanoparticles caused by the induced charge-transfer effect on intimate Au/g-C₃N₄ contact system, leading to more electrons being generated from the oxidation of BH₄⁻ (Eq. (3)), resulting in the enhanced catalytic activity of Au/g-C₃N₄ contact system.



On the basis of experimental results and the theoretical analysis, we propose a sequential three-step mechanism requiring six exogenous electrons for the reduction of *p*-nitrophenol to *p*-aminophenol on Au/g-C₃N₄ contact system (Scheme 1). As widely accepted, *p*-aminophenol is the only product of the six-electron reduction of *p*-nitrophenol in the presence of catalyst and excess NaBH₄ [55,56]. Therefore, reducibility of electron plays an essential role in nitrophenols hydrogenation reactions. In this work, Fermi level of Au NPs is close to the CB of g-C₃N₄ under visible light irradiation caused by the induced charge-transfer effect, which endue electrons with strong reducibility. In the reaction system, the BH₄⁻ was firstly oxidized to release of 6 electrons and H₂ on the Au

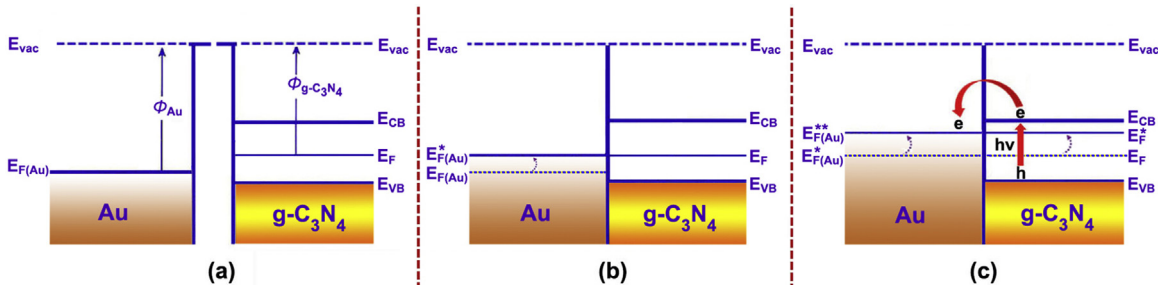


Fig. 7. The induced charge-transfer mechanism on intimate Au/g-C₃N₄ contact system: (a) before, (b) after Au and g-C₃N₄ contact, (c) after Au and g-C₃N₄ contact under visible light irradiation.

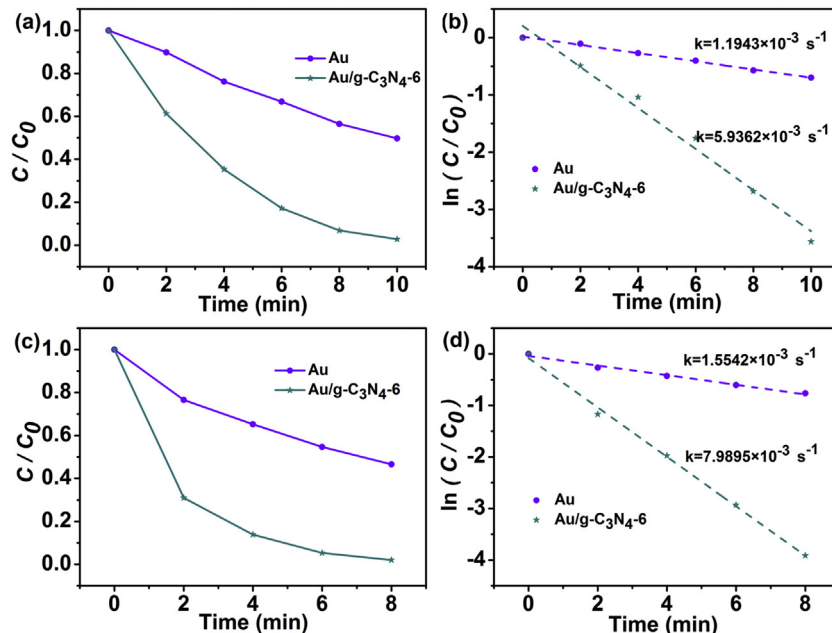


Fig. 8. Plots of C/C_0 versus reaction time and $\ln(C/C_0)$ versus reaction time for the catalytic reduction of *p*-nitrophenol to *p*-aminophenol over pure Au and Au/g-C₃N₄-6 contact system in the presence of NaBH₄ in the dark (a) and (b) and under visible light irradiation (c) and (d), respectively.

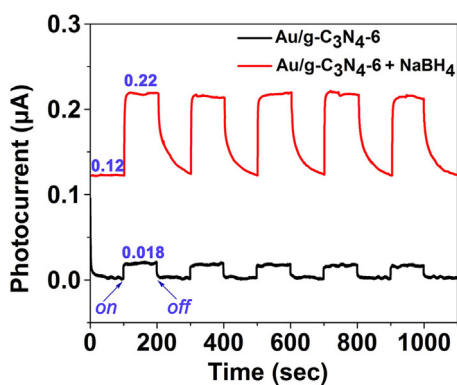
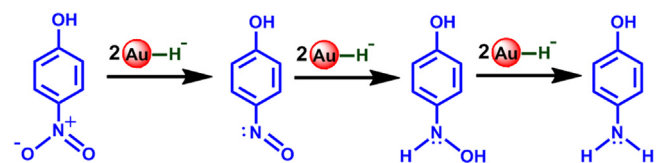


Fig. 9. Photocurrent transient responses of Au/g-C₃N₄-6 electrodes in 0.5 M Na₂SO₄ aqueous solution with 75 μ L of 0.1 g mL⁻¹ NaBH₄ aqueous solution and without NaBH₄.

nanoparticles (Eq. (3)), which can use two released electrons to activate H₂, forming negatively charged Au-H species with extremely high activity. In the presence of the Au-H species, *p*-nitrophenol (NO₂-Ar) can be reduced to aryl-nitroso (NO-Ar) in the first step, to aryl-dihydroxylamine (N(OH)₂-Ar) in the second step and to *p*-aminophenol (NH₂-Ar) in the final step. The whole reaction that the



Scheme 1. Sequential three-step reduction mechanism requiring six external electrons.

NO₂-Ar molecule can be converted to a NH₂-Ar molecule requires six active Au-H species, i.e. six exogenous electrons.

3. Conclusions

An intimate Au/g-C₃N₄ contact system with different Au contents has been fabricated via a simple one-step approach. Au NPs (2.6 nm) with narrow particle size distribution were firmly anchored on the surface of two-dimensional g-C₃N₄ sheets. The Au/g-C₃N₄ contact system displayed an unusual bi-functionality of catalytic and visible-light-driven photocatalytic activities for the reduction of nitrophenol to aminophenol, and therefore, a concerted catalysis was successfully achieved, which can be attributed to the negative shift in Fermi level of Au caused by the induced

charge-transfer effect due to the strong interaction between Au nanoparticles and g-C₃N₄.

Acknowledgements

This work was supported by NNSF of China (No. 51472120), China Postdoctoral Science Foundation (No. 2014M561651, No. 2015T80554), Jiangsu Planned Projects for Postdoctoral Research Funds (No. 1401003B), the Fundamental Research Funds for the Central Universities (No. 20915011311, No. 30916014103), the Opening Project of the Jiangsu Key Laboratory for Environment Functional Materials (No. SJHG1303), the Zijin Intelligent Program of NUST (2014) and PAPD of Jiangsu.

Appendix A. Supplementary data

Supplementary data associated with this article can be found, in the online version, at <http://dx.doi.org/10.1016/j.apcatb.2016.09.051>.

References

- [1] I.X. Green, W. Tang, M. Neurock, J.T. Yates, *Science* 333 (2011) 736–739.
- [2] M. Liu, R. Zhang, W. Chen, *Chem. Rev.* 114 (2014) 5117–5160.
- [3] N. Cheng, J. Tian, Q. Liu, C. Ge, A.H. Qusti, A.M. Asiri, A.O. Al-Youbi, X. Sun, *ACS Appl. Mater. Interfaces* 5 (2013) 6815–6819.
- [4] D. Preti, C. Resta, S. Squarcialupi, G. Fachinetti, *Angew. Chem. Int. Ed.* 50 (2011) 12551–12554.
- [5] P. Rodriguez, Y. Kwon, M.T.M. Koper, *Nat. Chem.* 4 (2012) 177–182.
- [6] Z.P. Jovanov, H.A. Hansen, A.S. Varela, P. Malacrida, A.A. Peterson, J.K. Nørskov, I.E.L. Stephens, I. Chorkendorff, *J. Catal.* (2016), <http://dx.doi.org/10.1016/j.jcat.2016.04.008>.
- [7] S.A. Nikolaev, E.V. Golubina, I.N. Krotova, M.I. Shilina, A.V. Chistyakov, V.V. Kriventsov, *Appl. Catal. B: Environ.* 168 (2015) 303–312.
- [8] C.W. Chiang, A. Wang, B.Z. Wan, C.Y. Mou, *J. Phys. Chem. B* 109 (2005) 18042–18047.
- [9] W. Zhu, S. Xiao, D. Zhang, P. Liu, H. Zhou, W. Dai, F. Liu, H. Li, *Langmuir* 31 (2015) 10822–10830.
- [10] M.O. Nutt, J.B. Hughes, M.S. Wong, *Environ. Sci. Technol.* 39 (2005) 1346–1353.
- [11] X.H. Li, M. Antonietti, *Chem. Soc. Rev.* 42 (2013) 6593–6604.
- [12] H.M.L. Davies, B.J. Du, J.Q. Yu, *Chem. Soc. Rev.* 40 (2011) 1855–1856.
- [13] S. Sarina, H. Zhu, E. Jaatinen, Q. Xiao, H. Liu, J. Jia, C. Chen, J. Zhao, *J. Am. Chem. Soc.* 135 (2013) 5793–5801.
- [14] B. Lim, H. Kobayashi, T. Yu, J. Wang, M.J. Kim, Z.Y. Li, M. Rycenga, Y. Xia, *J. Am. Chem. Soc.* 132 (2010) 2506–2507.
- [15] F. Gao, D.W. Goodman, *Chem. Soc. Rev.* 41 (2012) 8009–8020.
- [16] H.L. Jiang, T. Akita, T. Ishida, M. Haruta, Q. Xu, *J. Am. Chem. Soc.* 133 (2011) 1304–1306.
- [17] Y. Ma, W. Li, E.C. Cho, Z. Li, T. Yu, J. Zeng, Z. Xie, Y. Xia, *ACS Nano* 4 (2010) 6725–6734.
- [18] Q. Kang, T. Wang, P. Li, L. Liu, K. Chang, M. Li, J. Ye, *Angew. Chem. Int. Ed.* 54 (2015) 841–845.
- [19] M. Shekhar, J. Wang, W.S. Lee, W.D. Williams, S.M. Kim, E.A. Stach, J.T. Miller, W.N. Delgass, F.H. Ribeiro, *J. Am. Chem. Soc.* 134 (2012) 4700–4708.
- [20] E. Roze, P. Gravejat, E. Quinet, J.L. Rousset, D. Bianchi, *J. Phys. Chem. C* 113 (2008) 1037–1045.
- [21] X.Q. Deng, B. Zhu, X.S. Li, J.L. Liu, X. Zhu, A.M. Zhu, *Appl. Catal. B: Environ.* 188 (2016) 48–55.
- [22] J. Lee, J.C. Park, H. Song, *Adv. Mater.* 20 (2008) 1523–1528.
- [23] C. Zhu, L. Han, P. Hu, S. Dong, *Nanoscale* 4 (2012) 1641–1646.
- [24] J. Li, C. Liu, Y. Liu, *J. Mater. Chem.* 22 (2012) 8426–8430.
- [25] R. Wang, Z. Wu, C. Chen, Z. Qin, H. Zhu, G. Wang, H. Wang, C. Wu, W. Dong, W. Fan, J. Wang, *Chem. Commun.* 49 (2013) 8250–8252.
- [26] R. Kumar, E. Gravel, A. Hagège, H. Li, D.V. Jawale, D. Verma, I.N.N. Namboothiri, E. Doris, *Nanoscale* 5 (2013) 6491–6497.
- [27] T. Liu, F. Yang, Y. Li, L. Ren, L. Zhang, K. Xu, X. Wang, C. Xu, J. Gao, *J. Mater. Chem. A* 2 (2014) 245–250.
- [28] S. Wang, Q. Zhao, H. Wei, J.Q. Wang, M. Cho, H.S. Cho, O. Terasaki, Y. Wan, *J. Am. Chem. Soc.* 135 (2013) 11849–11860.
- [29] X. Liu, M. Conte, D. Elias, L. Lu, D.J. Morgan, S.J. Freakley, P. Johnston, C.J. Kiely, G.J. Hutchings, *Catal. Sci. Technol.* (2016), <http://dx.doi.org/10.1039/C6CY00090H>.
- [30] J. Saavedra, H.A. Doan, C.J. Pursell, L.C. Grabow, B.D. Chandler, *Science* 345 (2014) 1599–1602.
- [31] D. Ding, K. Liu, S. He, C. Gao, Y. Yin, *Nano Lett.* 14 (2014) 6731–6736.
- [32] I. Majeed, M.A. Nadeem, M. Al-Oufi, M. Arif Nadeem, G.I.N. Waterhouse, A. Badshah, J.B. Metson, H. Idriss, *Appl. Catal. B: Environ.* 182 (2016) 266–276.
- [33] X. Wang, K. Maeda, A. Thomas, K. Takanabe, G. Xin, J.M. Carlsson, K. Domen, M. Antonietti, *Nat. Mater.* 8 (2009) 76–80.
- [34] G. Algarra-Siller, N. Severin, S.Y. Chong, T. Björkman, *Angew. Chem.* 126 (2014) 7580–7585.
- [35] S. Cao, J. Low, J. Yu, M. Jaroniec, *Adv. Mater.* 27 (2015) 2150–2176.
- [36] X.H. Li, X.C. Wang, M. Antonietti, *Chem. Sci.* 3 (2012) 2170–2174.
- [37] J. Sun, Y. Fu, G. He, X. Sun, X. Wang, *Appl. Catal. B: Environ.* 165 (2015) 661–667.
- [38] Y. Fu, T. Huang, L. Zhang, J. Zhu, X. Wang, *Nanoscale* 7 (2015) 13723–13733.
- [39] Z. Zhang, C. Shao, P. Zou, P. Zhang, M. Zhang, J. Mu, Z. Guo, X. Li, C. Wang, Y. Liu, *Chem. Commun.* 47 (2011) 3906–3908.
- [40] M. Zhang, L. Liu, C. Wu, G. Fu, H. Zhao, B. He, *Polymer* 48 (2007) 1989–1997.
- [41] D. Jana, A. Dandapat, G. De, *Langmuir* 26 (2010) 12177–12184.
- [42] T. Huang, F. Meng, L. Qi, *J. Phys. Chem. C* 113 (2009) 13636–13642.
- [43] Y. Fu, J. Zhu, C. Hu, X. Wu, X. Wang, *Nanoscale* 6 (2014) 12555–12564.
- [44] N. Cheng, J. Tian, Q. Liu, C. Ge, A.H. Qusti, A.M. Asiri, A.O. Al-Youbi, X. Sun, *ACS Appl. Mater. Interfaces* 5 (2013) 10317–10324.
- [45] G. Ma, A. Binder, M. Chi, C. Liu, R. Jin, D. Jiang, J. Fan, S. Dai, *Chem. Commun.* 48 (2012) 11413–11415.
- [46] Y. Li, H. Wang, Q. Feng, G. Zhou, Z.S. Wang, *Energy Environ. Sci.* 6 (2013) 2156–2165.
- [47] C. Deraedt, L. Salmon, D. Astruc, *Adv. Synth. Catal.* 356 (11–12) (2016) 2525–2538.
- [48] S. Gazi, R. Ananthakrishnan, *Appl. Catal. B: Environ.* 105 (2011) 317–325.
- [49] X. Kong, Z. Sun, M. Chen, C. Chen, Q. Chen, *Energy Environ. Sci.* 6 (2013) 3260–3266.
- [50] E. Alberico, M. Nielsen, *Chem. Commun.* 51 (2015) 6714–6725.
- [51] V. Subramanian, E.E. Wolf, P.V. Kamat, *J. Phys. Chem. B* 107 (2003) 7479–7485.
- [52] M.T. Greiner, L. Chai, M.G. Helander, W.M. Tang, Z.H. Lu, *Adv. Funct. Mater.* 23 (2014) 215–226.
- [53] F. Yang, V. Kuznetsov, M. Lublow, C. Merschjann, A. Steigert, J. Klaer, A. Thomas, T. Schedel-Niedrig, *J. Mater. Chem. A* 1 (2013) 6407–6415.
- [54] B. Šljukić, J. Miličić, D.M. Santos, C.A. Sequeira, D. Macciò, A. Saccone, *J. Power Sources* 272 (2014) 335–343.
- [55] D. Bykov, F. Neese, *Inorg. Chem.* 54 (19) (2016) 9303–9316.
- [56] A.J. Komor, B.S. Rivard, R. Fan, Y. Guo, L. Que, J.D. Lipscomb, *J. Am. Chem. Soc.* (2016), <http://dx.doi.org/10.1021/jacs.6b03341>.